

Defects in irradiated silicon: EPR of the tin-vacancy pair

G. D. Watkins*

General Electric Corporate Research and Development, Schenectady, New York 12301

(Received 7 July 1975)

An EPR spectrum, labeled Si-G29, is identified as a lattice vacancy trapped by substitutional tin. The resulting tin-vacancy pair is observed in its neutral ground state with $S = 1$. Studies versus wavelength of illumination indicate that it has a donor level at $\sim E_v + 0.35$ eV. Analysis of the EPR spectrum leads to a model in which the tin atom resides in a position halfway between two normal silicon atom sites (D_{3d}). It is stable to ~ 500 K.

I. INTRODUCTION

Previous studies have demonstrated that lattice vacancies in silicon are mobile at temperatures well below room temperature.¹⁻³ When produced by radiation damage at cryogenic temperatures (4.2 and 20.4 K), isolated vacancies can be frozen and studied.¹⁻³ Upon warming (~ 70 K in n -type material; ~ 150 K in p -type material) the vacancies are observed to migrate through the lattice and are trapped by impurities and other defects to form more stable defect configurations. The configurations that have been identified include vacancies trapped by substitutional impurities (phosphorus,⁴ arsenic,⁵ antimony,⁵ boron,⁶ aluminum⁷), interstitial impurities (oxygen,^{8,9} chromium¹⁰), and other vacancies to form divacancies.^{1,11}

Vacancies can also be trapped by the isoelectronic impurity germanium. The resulting defect has been observed directly by electron paramagnetic resonance (EPR).¹² Its presence has also been inferred from the inhibiting effect of germanium on the formation of the oxygen-vacancy pair¹³ which can be monitored by its local-mode vibrational absorption in the infrared ($12 \mu\text{m}$).⁹ The germanium-vacancy binding energy is small, the defect breaking up at ~ 200 K.^{12,13} The consequent rerelease of vacancies has been observed as a growth in the $12\text{-}\mu\text{m}$ band as the vacancies in turn are trapped by oxygen.¹³

Brelot has reported similar effects in infrared studies of tin-doped silicon.^{14,15} Here, however, the $12\text{-}\mu\text{m}$ oxygen-vacancy band did not grow in until annealing to ~ 470 K. From this he inferred that tin-vacancy pairing also occurred and that the resulting defect was stable to ~ 470 K. Matsui *et al.*¹⁶ have also recently reported evidence of tin-defect pairing from Mössbauer studies of $^{119}\text{Sn}^m$ in neutron-irradiated silicon. In their work, isomer shifts and a quadrupole splitting revealed the presence of a defect next to the tin that anneals in the same temperature region as that observed by

Brelot. Two different configurations seemed to be indicated from their work, which they concluded to result from different charge states for the tin-vacancy pair.

In this paper we report the direct observation of the tin-vacancy pair by EPR. Annealing studies are described which confirm its stability. We thus confirm the interpretation of Brelot. In this paper we also describe the microscopic structure of the tin-vacancy pair, as deduced from its EPR spectrum. There are a number of unusual and interesting features.

II. EXPERIMENTAL PROCEDURE

EPR studies were performed at ~ 20 GHz and observed primarily at 20.4 and 4.2 K in dispersion. Two sets of samples were used, one doped with phosphorus ($\sim 10^{14}/\text{cm}^3$) and one doped with boron ($\sim 10^{16}/\text{cm}^3$). Both were grown by the inert gas floating-zone method and were doped with $\sim 3 \times 10^{18}/\text{cm}^3$ Sn by passing a final molten zone containing $\sim 2 \times 10^{20}/\text{cm}^3$ Sn through the sample.¹⁷ Irradiations were performed *in situ* at 20.4 K and also at room temperature with 1.5-MeV electrons from a resonant transformer accelerator.

Light was introduced to the sample via a hollow, gold-plated stainless-steel tube from outside the cryostat. The wavelength of light was controlled either by selective filters or by a $\frac{1}{4}$ -m Jarrell-Ash grating monochromator (295 lines/mm) with globar or tungsten source. Annealing studies were performed in a silicone oil bath.

III. EXPERIMENTAL RESULTS

A. General

Irradiation of tin-doped floating zone p -type silicon (Sn, $\sim 3 \times 10^{18}/\text{cm}^3$; B, $\sim 10^{16}/\text{cm}^3$) at 20.4 K with 1.5-MeV electrons produces the EPR spectra of isolated vacancies¹ and interstitial boron.¹⁸ Also present is a weak $S = 1$ spectrum which we label Si-G29. Upon annealing at ~ 180 K the vacancy

spectrum disappears and the Si-G29 spectrum grows correspondingly. This is illustrated in Fig. 1. The Si-G29 spectrum continues to increase somewhat versus anneal until it disappears at ~ 500 K.

In lightly irradiated *p*-type silicon where the Fermi level is still locked to the shallow acceptor boron ($\sim E_v + 0.05$ eV), the Si-G29 spectrum is seen only when the sample is illuminated with light. The dependence of the initial generation rate of the spectrum on the wavelength of the incident light is shown in Fig. 2. A threshold is indicated at $\lambda \sim 3.6 \mu\text{m}$, or $h\nu \sim 0.35$ eV. Identifying the process as reflecting a hole transition from the defect to the valence band suggests a corresponding electrical level position for the defect at $\sim E_v + 0.35$ eV, as shown.

The Si-G29 spectrum can also be produced in a room-temperature irradiation. Although accurate dosimetry was not performed, the production rate in a room-temperature irradiation appears to be a factor of 2 lower than that for 20.4 K irradiation and subsequent annealing to 300 K for the *p*-type material.

The Si-G29 spectrum is also observed in room-temperature irradiation of lightly doped *n*-type floating zone material ($\sim 10^{14}$ P/cm³), similarly doped with tin ($\sim 3 \times 10^{19}$ /cm³). In this material the Si-G29 spectrum is present in the dark, and is not enhanced by light.

B. Spectrum

The Si-G29 spectrum at 4.2 K is shown in Fig. 3, for $\vec{H} \parallel \langle 110 \rangle$. (The negative deflection for the low-field line is not due to level inversion effects, which have been reported for some photoexcited $S=1$ systems.^{7,19,20} Here it results simply because the energy level separation for this partic-

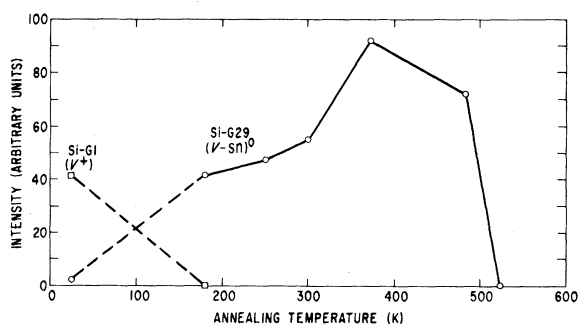


FIG. 1. Intensity of the Si-G29 spectrum vs 15-min isochronal anneal. The sample was *p*-type (boron, $\sim 10^{16}$ cm⁻³; tin, $\sim 10^{18}$ cm⁻³) and was irradiated at 20.4 K with 10^{17} electrons/cm² at 1.5 MeV.

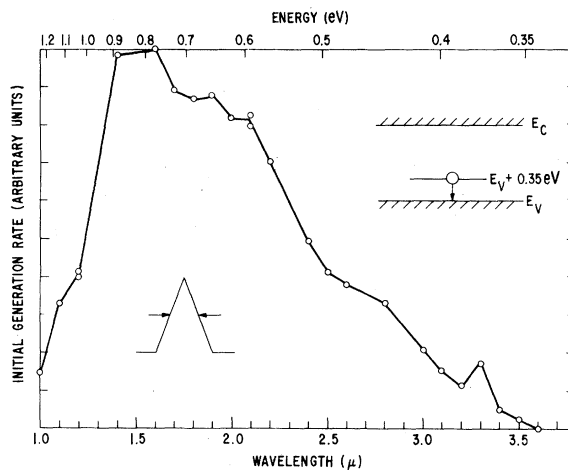


FIG. 2. Initial generation rate per unit energy of illumination of the Si-G29 spectrum in *p*-type material vs wavelength. The onset of generation at $3.5 \mu\text{m}$ identifies a level at $\sim E_v + 0.35$ eV, as shown.

ular transition decreases with increasing field, a consequence of the large fine-structure splitting associated with the spectrum.) The angular dependence of the lines is shown in Fig. 4. They range beyond the maximum field (14.5 kG) available from our magnet. (The small splitting of the lines at \vec{H} in the $[100]$ direction is due to a slight misalignment of the crystal, $\approx 2^\circ$.)

The spectrum can be described by the spin Hamiltonian

$$\mathcal{H} = \mu_B \vec{S} \cdot \vec{g} \cdot \vec{H} + D[S_z^2 - \frac{1}{3}S(S+1)] + \sum_j [\vec{S} \cdot \vec{A}_j - (\mu_j/I_j)\vec{H}] \cdot \vec{I}_j, \quad (1)$$

with $S=1$. The results of a computer fit for \vec{g} and D are given in Fig. 5. The spectrum is axially symmetric with the axis of symmetry (z') along a $\langle 111 \rangle$ axis of the crystal. The axes indicated in the figure are for one of the four equivalent defect orientations in the lattice. (The angular variation of

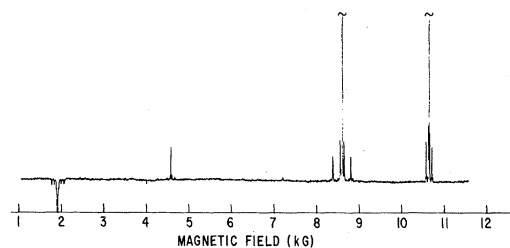


FIG. 3. Si-G29 spectrum at 20.4 K, $\vec{H} \parallel \langle 110 \rangle$, $\nu_0 = 20$ GHz.

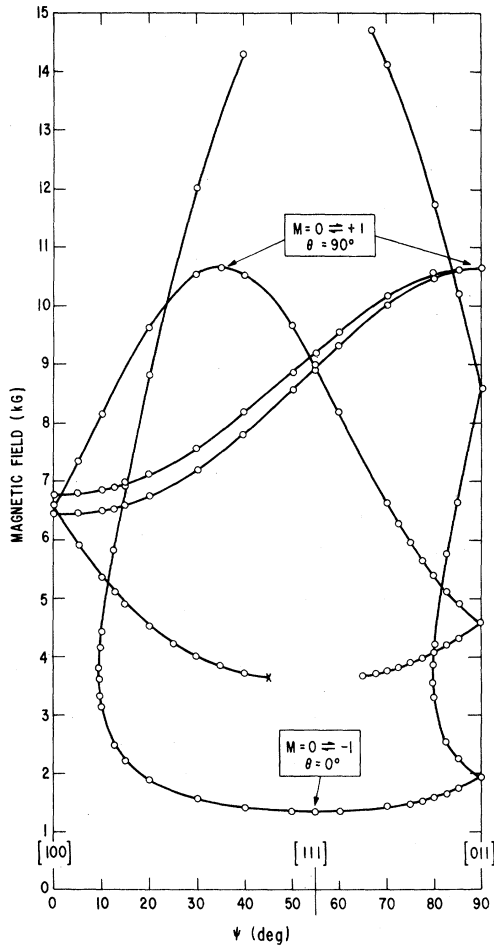
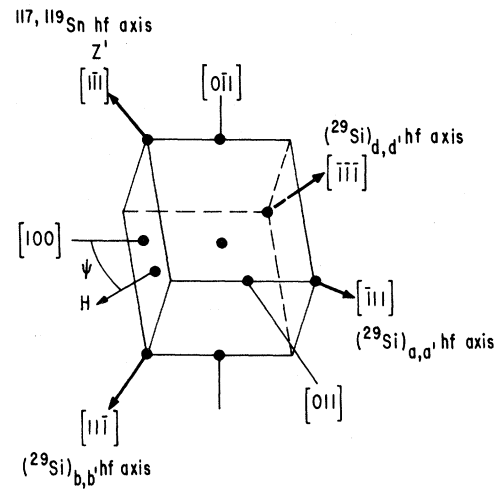


FIG. 4. Angular dependence of the Si-G29 spectrum with \vec{H} in the $[0\bar{1}1]$ plane. Here, θ is the angle between \vec{H} and the defect axis (ξ').

the spectrum in Fig. 4 appears different from the usual $S=1$ pattern in trigonal symmetry when $|D| < h\nu_0$.⁷ Here $|D| > h\nu_0$, and, as a result, fewer transitions are observed; some lines cannot be followed at all orientations of \vec{H} , etc. The analysis is straightforward, however, and we have identified some of the transitions in Fig. 4.)

Hyperfine interactions with the nuclear isotopes ^{117}Sn ($I = \frac{1}{2}$, 7.8% abundant), ^{119}Sn ($I = \frac{1}{2}$, 8.7%) and ^{29}Si ($I = \frac{1}{2}$, 4.7%) give rise to resolved satellites to the strong lines that can be seen in Figs. 3 and 6. The relative intensities of the satellites reveal that the interaction is with a single tin atom and with six silicon atoms which are equivalent in pairs. The principal values and axes for the hyperfine interactions, deduced from the angular dependence of the satellites, are also included in Fig. 5.

The sign of D was determined from the temper-



$$g_{\parallel} = 2.0107 \pm 0.0004 \quad {}^{119}\text{Sn} \begin{cases} A_{\parallel} = +124.8 \pm 1.0 (10^{-4} \text{ cm}^{-1}) \\ A_{\perp} = +131.0 \pm 1.5 (10^{-4} \text{ cm}^{-1}) \end{cases}$$

$$g_{\perp} = 2.0025 \pm 0.0005 \quad {}^{117}\text{Sn} \begin{cases} A_{\parallel} = +119.2 \pm 1.0 (10^{-4} \text{ cm}^{-1}) \\ A_{\perp} = +125.3 \pm 1.5 (10^{-4} \text{ cm}^{-1}) \end{cases}$$

$$D = +0.7988 \pm 0.0004 \text{ cm}^{-1}$$

$${}^{29}\text{Si} \begin{cases} A_{\parallel} = \pm 32.9 \pm 0.5 (10^{-4} \text{ cm}^{-1}) \\ A_{\perp} = \pm 22.7 \pm 0.5 (10^{-4} \text{ cm}^{-1}) \end{cases}$$

FIG. 5. Spin-Hamiltonian constants and relevant axes for one of the four equivalent defect orientations in the lattice.

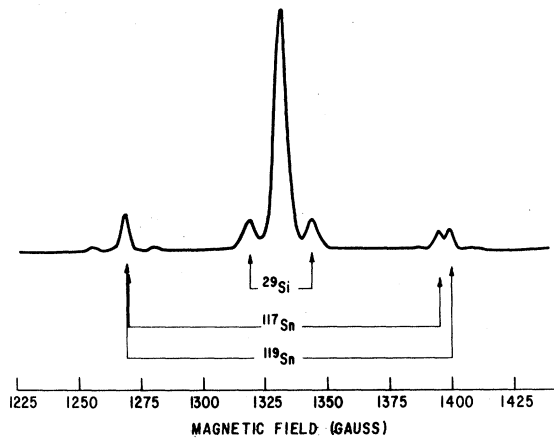


FIG. 6. $M=0 \rightarrow -1$ transition at $T=4.2 \text{ K}$, $\nu_0=20.2 \text{ GHz}$, with \vec{H} parallel to the $\langle 111 \rangle$ axis of symmetry ($\theta=0^\circ$, Fig. 4). Hyperfine satellites are indicated for ^{29}Si and $^{117,119}\text{Sn}$.

ature dependence of the relative intensities of the EPR transitions at 4.2 and 1.5 K. (The $\theta = 90^\circ$, $M=0 \rightleftharpoons +1$ transitions decreased in intensity at 1.5 K relative to the $\theta = 0^\circ$, $M=0 \rightleftharpoons -1$ transition, see Fig. 4. This reflects the Boltzmann population differences between the energy levels leading to a positive value for D .) The sign of the tin hyperfine interaction was determined directly from the positions of forbidden $\Delta m = 1$ hyperfine multiplets observed with $\vec{H} \parallel \langle 100 \rangle$. In this analysis the electronic wave functions were first determined by computer analysis. These were then used to solve for the nuclear part of the Hamiltonian, the last term in Eq. (1). A similar analysis has been described in Ref. 7.

The signs for the ^{29}Si hyperfine interactions could not be determined.

C. Isotope shifts in D

The ^{117}Sn and ^{119}Sn hyperfine multiplets are approximately superposed on the low-field side of Fig. 6 but are well resolved on the high-field side. This reveals that the centers of gravity for the two are different. We interpret this as a slight shift in D due to the differing isotopes of tin. Careful analysis, including small second-order corrections in $A/g\mu_B H$, give $\delta D/D = +1.0 \times 10^{-4}$ per unit mass change of the tin atom. The ^{29}Si satellites are also shifted with respect to the central line revealing $\delta D/D = -0.67 \times 10^{-4}$ per unit mass for each silicon neighbor.

Fractional shifts in D of this order have been previously reported for Cr^{3+} in MgO ,²¹ and Fe^{3+} in calcite.²² There the resulting shifts in the line positions were ≤ 0.1 G and difficult to detect. In the Si-G29 spectrum they are more evident because of the larger value of D and also because the lines remain narrow, a property of the high crystalline perfection of silicon. It must still be considered remarkable that such effects, which have been reported in only two other cases, should be so evident for an atom as heavy as tin.

We have previously reported these results²³ and we will not discuss them in detail here. In this previous communication we pointed out also that the shape and breadth of the central line is adequately described by the isotope shifts of the many nonmagnetic isotopes of tin (112–124). We postulated that the shifts were vibrational in origin and showed that the low-temperature values were consistent with the zero-point vibrational amplitudes associated with a vibrational frequency for the tin atom of $\sim 50 \text{ cm}^{-1}$, a reasonable value.

D. Effects of stress

Uniaxial stress of 1700 kg/cm^2 was applied to a $\langle 110 \rangle$ axis of the crystal at 185°C for 15 min and

then the sample was cooled to room temperature with stress on. The stress was then removed and the sample placed in the EPR cavity for observation at 20.4 K . A preferential alignment of the defects was found to have been frozen in, as measured by the relative intensities of the corresponding spectral lines. The defects whose $\langle 111 \rangle$ axes were perpendicular to the stress directions were decreased in intensity; the defects whose $\langle 111 \rangle$ axes were 35.3° from the $\langle 110 \rangle$ stress direction were increased. The results are shown in Fig. 7 along with the disappearance of the alignment *versus* 15-min isochronal anneals.

IV. DISCUSSION

A. Model

The 1:1 growth of the Si-G29 spectrum as the vacancy spectrum disappears leads us to conclude that it is to be identified as a tin-vacancy pair. A model consistent with the EPR results is shown in Fig. 8. Here the tin atom is located halfway between two normal silicon-atom sites. In this position it is equidistant from six silicon atoms (a, a', b, b', d, d') which form a distorted octahedron around the tin atom. In this position the six atoms are equivalent by pairs (unprimed and primed inversion pairs) explaining the corresponding equivalence in the silicon hyperfine interactions.

In Fig. 9 we present a simple ligand-field molecular-orbital model for the defect. Here the central tin atom $5s$, $5p$, and $5d$ orbitals interact with the ligand orbitals, which are made up as linear combinations of a single dangling orbital from each of the six silicon neighbors. We show (a) the orbitals in octahedral (O_h) symmetry; (b) in $\langle 111 \rangle$ distorted

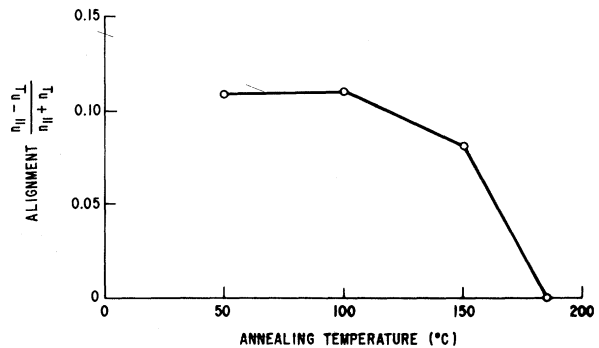


FIG. 7. A 15-min isochronal annealing study of the stress-induced alignment of the defect (z') axis. Alignment was initially achieved by applying 1700 kg/cm^2 stress at 185°C and cooling to room temperature with stress on.

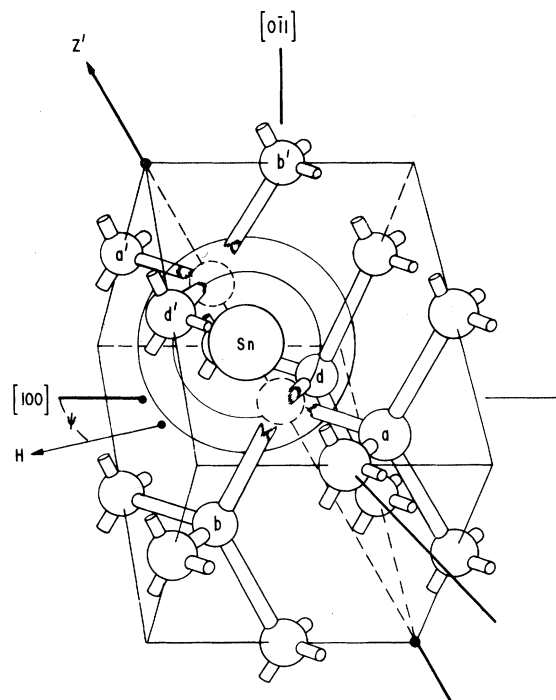


FIG. 8. Model for the tin-vacancy pair. The tin atom is halfway between two normal silicon-atom sites, equidistant from the six silicon atoms labeled a , a' , b , b' , d , d' .

octahedral (D_{3d}) symmetry; and (c) the result of overlap and admixture. We note that viewed this way the defect can be considered a tin atom in the center of a "divacancy," the separated ligand orbitals in D_{3d} corresponding to those previously treated for the divacancy.^{11,24}

Filling the orbitals with ten electrons corresponds to the neutral state for the defect. The last two electrons in the e_g orbital have their spins parallel leading to an orbitally nondegenerate $S=1$ (${}^3A_{2g}$) ground state and, therefore, no Jahn-Teller distortion.

In this model the filled electronic orbitals derive primarily from the "divacancy" ligand orbitals of the six silicon neighbors, which have been "stabilized" by the presence of the tin atom. They have partial tin character via their admixtures [$5s$ in a_{1g} , $5p_z$ in a_{2u} , $5p_{x',y'}$ in e_u , and $5d$ (e_g) in e_g].

B. Hyperfine interactions

Following the procedure used in the study of previous centers,^{4,5} we may analyze the hyperfine interactions, in terms of one-electron wave functions, which are linear combinations of atomic orbitals centered on the atoms near the defect.

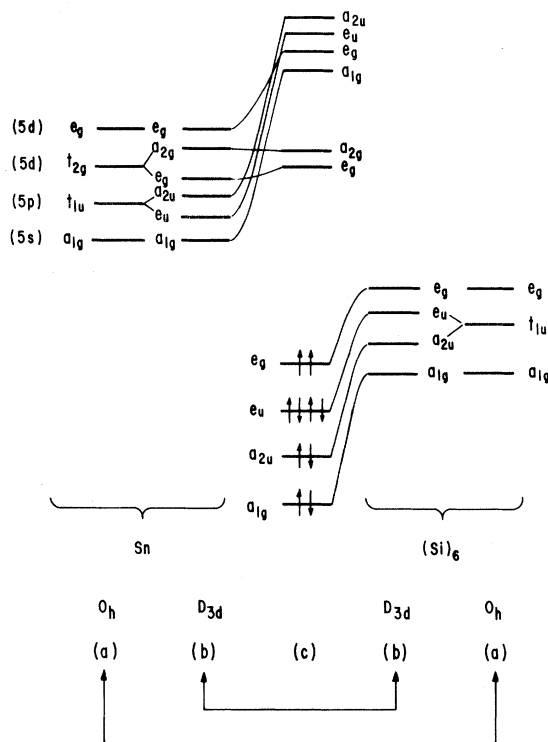


FIG. 9. Simple molecular-orbital model for the defect: (a) The central tin atom and ligand orbitals in octahedral O_h symmetry; (b) The corresponding orbitals in the distorted octahedral symmetry (D_{3d}) of the defect; (c) The molecular orbitals resulting from overlap and mixture of the ligand and central tin-atom orbitals.

Using estimates of $\langle r^{-3} \rangle_{3p}$ and $|\psi^2(0)|_{3s}$ previously estimated for silicon,⁴ we deduce that each of the six silicon atoms accounts for $\sim 12\%$ of the total wave function, and on each the wave function is $\sim 16\%$ $3s$ and $\sim 84\%$ $3p$. Therefore, $\sim 72\%$ of the wave function is accounted for on these atoms.

The magnetic moments of the tin isotopes are negative. The observed positive hyperfine interaction implies, therefore, a *negative* spin density at the nucleus, which in turn implies an indirect interaction (configuration interaction,²⁵ exchange polarization,²⁶ etc.). With $|\psi^2(0)| = 116(10^{24})$ for the $5s$ orbital,²⁷ the isotropic part of the tin hyperfine interaction could be produced by $\sim 1\%$ $5s$ character. For an inner shell the amount required would be significantly less.

We conclude, therefore, that most of the wave function is on the six silicon neighbors with a relatively small admixture of e_g ($5d$) tin orbitals.

C. \bar{g} and D

Spin-orbit interaction with the $5d$ orbitals on the tin atom should produce a negative component to

the g shift, the excitations from the e_g ($5d$) orbitals being to higher-energy one-electron t_{2g} orbitals, as seen in Fig. 9. The observed g shifts, however, are positive, which would appear to rule out a dominant contribution from these excitations. This is consistent with our hyperfine analysis which indicated only a small percentage of the wave function on the tin.

On the other hand, positive g shifts of the observed magnitude can be accounted for in terms of spin-orbit interactions on the silicon neighbors. In particular, we have previously shown⁴ that the g shift associated with an electron in a single dangling silicon bond is $\sim \Delta g'_{\parallel} \sim 0$, $\Delta g'_{\perp} \sim +0.01 - 0.02$, where "parallel" and "perpendicular" refer to the dangling bond axis. Ignoring overlap between the dangling bonds and interactions between the electrons, these one-electron contributions averaged over the six silicon neighbors predict g shifts of the correct magnitude with $\Delta g_{\parallel} > \Delta g_{\perp}$, as observed. (This analysis⁷ predicts $\Delta g_{\parallel}/\Delta g_{\perp} = \frac{8}{5}$, overestimating Δg_{\perp} . The model must be considered, therefore, considerably oversimplified. It is possible, for instance, that small negative g -shift components from the $5d$ excitations on the tin could reduce both Δg_{\perp} and Δg_{\parallel} so that $\Delta g_{\perp} \sim 0$, as observed.)

The fine-structure term D is almost two orders of magnitude larger than can be accounted for by dipole-dipole interactions averaged over the wave function on the silicon neighbors. (A typical value for a divacancy is $\sim 0.01 \text{ cm}^{-1}$.²⁸) In a previous study on a similar $S = 1$ center, the aluminum-vacancy pair,⁷ we showed that large values of D , such as observed here, can arise through spin-orbit interaction. There we found that the relationship

$$D_{ij} = -\frac{1}{2}\lambda\Delta g_{ij} \quad (2)$$

derived by Pryce²⁹ for an ion in Russell-Saunders coupling (spin-orbit interaction among states derived from the same atomic term, i.e., same L and S) predicted the correct magnitude for D .

Applying the same arguments to the tin-vacancy pair with $g_{\parallel} - g_{\perp} = +0.0072$ and $\lambda = -0.02 \text{ eV}$ (the magnitude is that for atomic silicon; the sign comes from the fact that the g shifts are positive), we obtain

$$D = D_{\parallel} - D_{\perp} \sim -0.6 \text{ cm}^{-1}.$$

Here, again, the magnitude is correct. However, the sign is wrong. (In our previous study on the aluminum-vacancy pair, the sign of D could not be determined experimentally because the $S = 1$ state was an excited state. It is possible, therefore, that the predicted sign in that case was also in error.)

The use of Eq. (2), of course, cannot be easily justified for such a center. This is a diffuse many-center molecular wave function and there are many atomic and molecular excited states available that do not fit into the simple Russell-Saunders scheme used to derive (2). In particular, there are apt to be low-lying singlet states (the $^1A_{1g}$ and 1E_g made up from the same e_g^2 configuration) which can be coupled to the ground $^3A_{2g}$ state via spin-orbit interaction. Although matrix elements to these states are apt to be weak, their proximity in energy could make their contributions significant. These could contribute either sign to D but simple arguments suggest that the dominant coupling is apt to arise between $^3A_{2g}(M=0)$ and $^1A_{1g}(M=0)$ which provides a positive sign for D .

We conclude that spin-orbit interaction probably provides the origin of D but that a detailed treatment would be very difficult.

D. Stress alignment

The energy of a defect in an applied strain field can be written

$$E = \sum_{i,j} B_{ij}\epsilon_{ij}, \quad (3)$$

where ϵ_{ij} are the strain tensor components and B_{ij} are the components of a symmetric second-rank "piezospectroscopic"³⁰ tensor \vec{B} . Kaplyanski³⁰ has shown that for a center of trigonal ($\bar{1}11$) symmetry, \vec{B} has the form

$$\vec{B} = \begin{pmatrix} -B + B_0 & 0 & 0 \\ 0 & -B + B_0 & 0 \\ 0 & 0 & +2B + B_0 \end{pmatrix}, \quad (4)$$

where the 3-axis is the z' trigonal axis of the defect. We equate the stress-induced alignment

$$n_{\parallel}/n_{\perp} = \exp[-(E_{\parallel} - E_{\perp})/kT], \quad (5)$$

where E_{\parallel} and E_{\perp} are given by (3) for each defect orientation and T is the temperature of the equilibrium alignment.

For stress $\sigma(0\bar{1}1)$ along the $[0\bar{1}1]$ direction, Eqs. (3) and (4) lead to

$$B = \frac{E_{\parallel} - E_{\perp}}{S_{44}\sigma(0\bar{1}1)}, \quad (6)$$

where S_{44} is the shear elastic modulus of silicon ($= 12.56 \times 10^{-13} \text{ cm}^2/\text{dyn}$).³¹ With $n_{\parallel}/n_{\perp} \approx 1.25$ and $T \approx 170 \text{ }^\circ\text{C}$ (Fig. 7), we obtain

$$B \approx +4.1 \text{ eV}/(\text{unit strain}).$$

The positive sign means that the energy of the defect is lowered if compressed along its $(\bar{1}11)$ trigonal axis. This is reasonable in terms of the

model of Fig. 8 in that the resulting distortion increases the overlap of the tin orbitals with those on the six silicon neighbors and makes the symmetry closer to octahedral. (This is of the opposite sign from that observed for the photo-excited $S=1$ state of the aluminum-vacancy pair.⁷ There it was postulated that the coupling was dominated by a Jahn-Teller distortion in its 1E ground state. The ground state for the tin-vacancy pair is ${}^3A_{2g}$ and no Jahn-Teller distortions occur.)

Thermally activated reorientation occurs at $\sim 160^\circ\text{C}$. As noted for other impurity-vacancy pairs, reorientation of the defect requires that the vacancy make two diffusioned jumps away from the impurity and then return.^{4,5,7} The activation energy for reorientation thus includes a term arising from the difference in the binding energy between the defect in its ground configuration and with the vacancy separated to the next-nearest position. This binding for the tin-vacancy pair is, therefore, greater than for the group-V-vacancy pairs (reorient at ${}^{4,5} \sim 20\text{--}85^\circ\text{C}$) but less than the aluminum-vacancy pair ($\sim 250^\circ\text{C}$)⁷. The annealing of the defect at $\sim 225^\circ\text{C}$ is also intermediate between that for the other centers.

V. SUMMARY AND CONCLUSIONS

Substitutional tin is an effective trap for lattice vacancies. The tin-vacancy pair which results appears to produce a single-donor level at $\sim E_v + 0.35$ eV (Fig. 2). Spin resonance in the single-positive-charge state was not observed. In the neutral state the ground state is a triplet ($S=1$) and the EPR has been reported in this paper. The defect is stable to ~ 500 K.

The configuration is one in which the tin atom resides in the D_{3d} position halfway between two normal silicon-atom sites. Although many vacancy-impurity centers have been studied previously, this is the first center observed with this configuration. We presume that this is because tin is a large, heavy atom, its valence orbitals overlapping significantly all of the six silicon neighbors in this position. In addition, the low-lying $5d$ orbitals provide additional angular-momentum states around the central tin atom that allow a bonding role for all ten electrons in the distorted octahedral complex. (In terms of hybridized-bonding concepts,³² the sp^3d^2 orbitals can form six octahedrally directed bonding orbitals on the central atom.)

This configuration is similar to one considered by Masters³³ for the isolated vacancy. He argued that one of the four neighbor silicon atoms might move into the D_{3d} site halfway between two atom sites and form what he called a "semivacancy

pair." His arguments also included the possible role of $3s(3p)^3(3d)^2$ hybridization on the central silicon atom. Our results for tin illustrate that his concepts were valid ones. However, silicon is apparently too small, as is germanium, the EPR studies of the isolated lattice vacancy and the germanium-vacancy pair indicating the atoms to be in the normal lattice sites.

We can consider the large tin atom as moving into this position because it can successfully bond with all six of the silicon neighbors. As such, it is attempting to "heal" all of the ruptured bonds associated with a lattice vacancy.

Unfortunately, it does not completely heal the vacancy because there remains an electrical level at $\sim E_v + 0.35$ eV. From a technological standpoint, it would have been valuable if the healing had been complete. This points up the possibility that a heavier isoelectronic impurity such as lead might serve this purpose. This prospect should be explored.

Another interesting property of the center is that its ground state is a triplet $S=1$ state (${}^3A_{2g}$). A number of $S=1$ EPR centers have previously been observed in irradiated silicon. These include excited states of centers derived from single vacancies (oxygen-vacancy²⁰ and aluminum-vacancy⁷ pairs) and ground states of centers believed to be associated with more diffuse multiple-vacancy centers.^{28,34} The tin-vacancy pair is the first center derived from the single vacancy which is observed to have its ground state $S=1$.

For single-vacancy centers, we have previously argued that Jahn-Teller effects tend to be strong and override the electron-electron interactions which might otherwise favor the higher multiplicity states.^{5,35,36} The tin-vacancy pair represents a departure from this rule. In particular, if two electrons had gone into a single e_g orbital, and paired off (see Fig. 9) forming a 1E_g state, then a Jahn-Teller distortion could have occurred. Apparently, however, the potential Jahn-Teller energy gain from the 1E_g state is not sufficient to override the initial ${}^3A_{2g}$ - 1E_g energy difference. The reason for this difference in behavior is not clear. It is possible that the tin atom plays an important direct role, but the low spin density of the e_g orbitals on the tin make this unlikely. Perhaps the principal role of the tin in the center is to force the e_g wave function over the six silicon atoms and make it more diffuse.

The presence of a small concentration of tin-vacancy pairs before annealing (Fig. 1) indicates that some migration of vacancies is taking place during the 20.4 K irradiation. This has previously been noted for germanium-vacancy pairing and for oxygen-vacancy pairing.³ Recent studies with 1.06-

μm laser illumination at 20.4 K have confirmed that migration of vacancies can be produced at this temperature by ionization.⁶ Presumably the ionization accompanying the electron irradiation causes the migration.

Finally, our observation that two charge states exist for the tin-vacancy pair is consistent with the conclusion of Matsui *et al.*¹⁶ from Mössbauer studies. Hopefully, the detailed model that we have

presented in this paper for the neutral charge state of the defect will prove helpful in sorting out the quadrupole splittings and isotope shifts observed by these workers.

ACKNOWLEDGMENT

The assistance of L. A. Gruenke in all phases of the measurements is gratefully acknowledged.

*Present address: Dept. of Physics, Lehigh University, Bethlehem, Pa. 18015

¹G. D. Watkins, J. Phys. Soc. Jpn. Suppl. II **18**, 22 (1963).

²G. D. Watkins, in *Radiation Damage in Semiconductors* (Dunod, Paris, 1965), p. 97.

³G. D. Watkins, in *Lattice Defects in Semiconductors 1974* (Institute of Physics, London, 1975), p. 1.

⁴G. D. Watkins and J. W. Corbett, Phys. Rev. **134**, A1359 (1964).

⁵E. L. Elkin and G. D. Watkins, Phys. Rev. **174**, 881 (1968).

⁶G. D. Watkins (unpublished).

⁷G. D. Watkins, Phys. Rev. **155**, 802 (1967).

⁸G. D. Watkins and J. W. Corbett, Phys. Rev. **121**, 1001 (1961).

⁹J. W. Corbett, G. D. Watkins, R. M. Chrenko, and R. S. McDonald, Phys. Rev. **121**, 1015 (1961).

¹⁰H. H. Woodbury and G. W. Ludwig, Phys. Rev. Lett. **5**, 96 (1960).

¹¹G. D. Watkins and J. W. Corbett, Phys. Rev. **138**, A543 (1965).

¹²G. D. Watkins, IEEE Trans. Nucl. Sci. **NS-16**, 13 (1969).

¹³A. Brelet and J. Charlemagne, in *Radiation Effects in Semiconductors*, edited by J. W. Corbett and G. D. Watkins (Gordon and Breach, New York, 1971), p. 161.

¹⁴A. Brelet, in *Radiation Damage and Defects in Semiconductors*, edited by J. E. Whitehouse (Institute of Physics, London, 1973), p. 191.

¹⁵A. Brelet, IEEE Trans. Nucl. Sci. **NS-19**, 220 (1972).

¹⁶K. Matsui, R. R. Hasiguti, T. Shoji, and A. Ohkawa, in Ref. 3, p. 572.

¹⁷Specially grown by High Performance Technology, Inc. Midland, Mich.

¹⁸G. D. Watkins, Phys. Rev. B (to be published).

¹⁹H. Tanimoto, W. M. Zinker, and J. O. Kemp, Phys. Rev. Lett. **14**, 645 (1965).

²⁰K. L. Brower, Phys. Rev. **134**, 1968 (1971).

²¹S. A. Marshall, J. A. Hodges, and R. A. Serway, Phys. Rev. **136**, A1024 (1964).

²²S. A. Marshall, J. A. Hodges, and R. A. Serway, Phys. Rev. **133**, A1427 (1964).

²³G. D. Watkins, Solid State Commun. (to be published).

²⁴Note that in Ref. 11 we incorrectly labeled the a_{2u} state as a_{1u} in D_{3d} .

²⁵A. Abragam, J. Horowitz, and M. H. L. Pryce, Proc. R. Soc. A **230**, 169 (1955).

²⁶J. H. Wood and G. W. Pratt, Jr., Phys. Rev. **107**, 995 (1957).

²⁷F. Herman and S. Skillman, *Atomic Structure Calculations* (Prentice-Hall, Englewood Cliffs, N. J., 1963).

²⁸K. L. Brower, in *Radiation Effects in Semiconductors*, edited by J. W. Corbett and G. D. Watkins (Gordon and Breach, New York, 1971), p. 189.

²⁹M. H. L. Pryce, Proc. Phys. Soc. Lond. A **63**, 25 (1950).

³⁰A. A. Kaplyanskii, Opt. i. Spektrosk. **16**, 602 (1964); [Opt. Spectry. (USSR) **16**, 329 (1964)].

³¹H. B. Huntington, in *Solid State Physics*, edited by F. Seitz and D. Turnbull (Academic, New York, 1958), Vol. 7, p. 274.

³²L. Pauling, *The Nature of the Chemical Bond* (Cornell U. P., Ithaca, N. Y., 1948), 2nd ed., Chap. 3.

³³B. J. Masters, Solid State Commun. **9**, 283 (1971).

³⁴J. W. Corbett, *Electron Radiation Damage in Semiconductors and Metals* (Academic, New York, 1966), p. 79ff.

³⁵G. D. Watkins, in *Radiation Effects in Semiconductors*, edited by F. L. Vook (Plenum, New York, 1968), p. 67.

³⁶G. D. Watkins, in Ref. 14, p. 228.